Available online at www.sciencedirect.com
SCIENCE DIRECT®
Journal of Solid State Chemistry 178 (2005) 2811–2817
JOURNAL OF SOLID STATE CHEMISTRY
www.elsevier.com/locate/jssc

Extension of the $La_7Mo_7O_{30}$ structural type with $La_7Nb_3W_4O_{30}$ and $La_7Ta_3W_4O_{30}$ compounds

F. Goutenoire[a,*], S. Kodjikian[a], E. Suard[b]

[a] *Laboratoire des Oxydes et Fluorures, UMR-CNRS 6010, Université du Maine, 72085 Le Mans cedex 9, France*
[b] *Institut Laue Langevin, Avenue des Martyrs, B.P 156, 38042 Grenoble Cedex 9, France*

Received 6 April 2005; received in revised form 13 June 2005; accepted 15 June 2005
Available online 28 July 2005

Abstract

Two compounds of formula $La_7A_3W_4O_{30}$ (with A = Nb and Ta) were prepared by solid-state reaction at 1450 and 1490 °C. They crystallize in the rhombohedric space group R-3 (No. 148), with the hexagonal parameters: $a = 17.0640(2)$ Å, $c = 6.8859(1)$ Å and $a = 17.0701(2)$ Å, $c = 6.8851(1)$ Å. The structure of the materials was analyzed from X-ray, neutron and electronic diffraction. These oxides are isostructural of the reduced molybdenum compound $La_7Mo_7O_{30}$, which are formed of perovskite rod along [111]. An order between (Nb, Ta) and W is observed.

Keywords: Perovskite; X-ray and neutron diffraction; Electron microscopy; BVS

1. Introduction

Oxide ion conductors still attract attention due to their potential application in solid-oxide fuel cell. These oxides belong to only a few number of structural families [1]: fluorite type (stabilized zirconia, δ-Bi_2O_3), perovskite (doped $LaGaO_3$, $Ba_2In_2O_5$), intergrowth perovskite/Bi_2O_2 slabs (BIMEVOX) and pyrochlore ($Gd_2Ti_2O_7$). More recently, new structural types have shown good oxide ion conduction. We can cite our work on $La_2Mo_2O_9$ [2,3] which has no structural relation to any other structural type or the more conventional Apatite structure $La_{9.33}Si_6O_{26}$ [4].

As an extension to the stabilized zirconia, solid-state chemists have explored structures related to fluorite type, mainly the Scheelite structure. Some recent works on $Pb_{1-x}La_xW_{4+x/2}$ [5,6], $CeTaO_4$ [7] and $BiVO_4$ [8] have been reported. But attention to related Scheelite structure is even more ancient compared with the work on excess Scheelite-based compounds $La_{1-x}Th_xNbO_{4+x/2}$ and $LaNb_{1-x}W_xO_{4+x/2}$ examined by Cava et al. [9]. From this study a compound of formula $LaNb_{0.4}W_{0.6}O_{4.3}$ was reported without structural information's.

Here, we present the synthesis, physical and structural characterization of two new phases with the formula $La_7Nb_3W_4O_{30}$ and $La_7Ta_3W_4O_{30}$, which are isostructural of the reduced molybdate phases $La_7Mo_7O_{30}$ [10].

2. Experimental

The room temperature and thermal X-ray diffraction patterns were collected on a Bragg-Brentano diffractometer (MPD-PRO Panalytical) equipped with a linear detector X'Cellerator and an Anton Paar HTK12 furnace. For the structural analysis, the diffraction pattern was collected in the range (10°–145° (2θ)), with an increment step of 0.017° (2θ) and a total collecting time of 5.33 h. The thermal X-ray diffraction patterns were collected during one night. The neutron diffraction

*Corresponding author. Fax: +33 2 43 83 35 06.
E-mail address: goutenoire.francois@univ-lemans.fr (F. Goutenoire).

0022-4596/$ - see front matter © 2005 Elsevier Inc. All rights reserved.
doi:10.1016/j.jssc.2005.06.020

patterns of $La_7Ta_3W_4O_{30}$ and $La_7Nb_3W_4O_{30}$ were collected on the Debye-Sherrer diffractometer D1A (instrument at ILL, Grenoble). Data collection was performed at ~1.911 Å on ~15 g of compound. For the patterns the increment step was 0.05° (2θ), interval of data collection ranging from 0° to 162°, the total counting time was ~6 h for $La_7Ta_3W_4O_{30}$ and ~2 h for $La_7Nb_3W_4O_{30}$.

The electron diffraction study was performed on a 200 kV side entry JEOL2010 transmission electron microscope with a double-tilt specimen holder operating at room temperature. For specimen preparation, a small amount of powder was ground in an agate mortar and pestle under dry methanol to produce a suspension. A drop of the suspension was deposited on a holey carbon film supported by a 1000 mesh copper grid and dried.

The density measurements were carried out on a gas pycnometer ACCUPIC 1330 (Micromeritics) with helium as gas. The temperature of measurement was 24 °C ± 1 °C, for each measurement an amount of approximately 200 mg was used.

The transport property was studied by impedance spectroscopy using a Schlumberger Solartron SI 1260 frequency response analyzer with 0.1 V amplitude signal over the 32 MHz–0.1 Hz frequency range. Pellets of 10 mm diameter were used for measurements with, as electrodes, platinum deposited on both faces.

3. Results and discussion

3.1. Synthesis

Different compounds were prepared with La_2O_3, Nb_2O_5 and Ta_2O_5 and WO_3 as starting oxides. Lanthanum oxide powder was dried and decarbonated at 1000 °C overnight prior to use. The first attempt of synthesis was done with the nominal composition $LaNb_{0.4}W_{0.6}O_{4.3}$ as mentioned by Cava et al. [9] at 1400 °C for one night (see Fig. 1). The same five strongest lines were obtained in the powder pattern: $d = 4.263$, 3.221, 2.928, 2.637 and 1.984 Å. The structure is isotypic with $La_7Mo_7O_{30}$, this feature was found after the electron diffraction analysis. Nevertheless, both the compositions are closed, the compound $LaNb_{0.4}W_{0.6}O_{4.3}$ presents 60 mol% of $LaWO_{4.5}$ and $La_7Nb_3W_4O_{30}$ presents 57.1 mol% of $LaWO_{4.5}$. Subsequently, $La_7A_3W_4O_{30}$ (with A = Nb and Ta) compounds were synthesized from the stoichiometric composition of oxides. The weighted powders were ground in an agate mortar for few minutes and then placed in an alumina crucible. Finally, the powders were heated for one night at 1450 °C and 1490 °C, respectively, for $La_7Nb_3W_4O_{30}$ and $La_7Ta_3W_4O_{30}$; no particular condition was used in order to cool down the samples. The final compounds were obtained in white color.

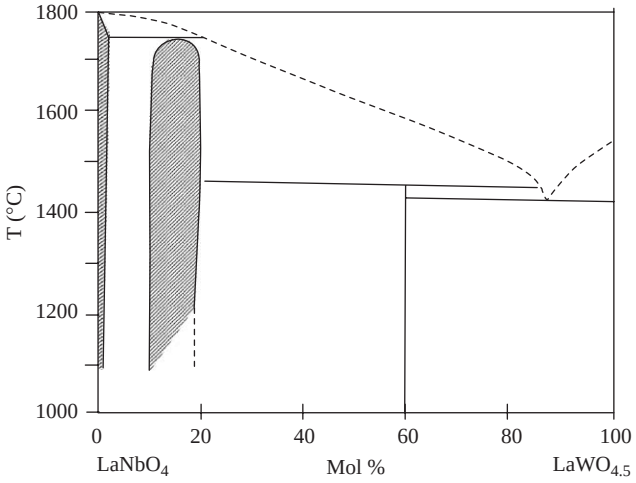

Fig. 1. Phase equilibrium diagram for the system $LaNbO_4$–$LaWO_{4.5}$ (from Ref. [9], solid solution domain is hatched for clarity).

3.2. Electron diffraction and high resolution electron microscopy

As for the analysis of $La_7Mo_7O_{30}$ [10], the first reciprocal lattice reconstruction, performed by electron diffraction, which allowed us to determine the cell parameters in the wrong monoclinic subcell was as follows:

$$a \approx 10.4,\ b \approx 17.2,\ c \approx 6.6,\ \text{and}\ \beta \approx 110°.$$

The observed reflection condition during the reciprocal lattice reconstructions was hkl: $h + k = 2n$, leading to the monoclinic space groups: $C2/m$. The true hexagonal lattice was deduced from the observation of electron diffraction pattern along the [001]* hexagonal cell as shown in Fig. 2, and from our previous experience. No extra reflection dots involving the doubling of the c parameter was observed, this was also the case in $La_7Mo_7O_{30}$ electron diffraction analysis. High-resolution electron microscopy images were measured along [001] direction, a very periodic contrast was observed in the whole crystal attesting of the nice ordering of the structure (Fig. 3). The same feature was also evidenced in the $La_7Mo_7O_{30}$ compound.

3.3. Refinement and structure analysis

The first structural refinements on the both $La_7Ta_3W_4O_{30}$ and $La_7Nb_3W_7O_{30}$ were analyzed by combining X-rays and neutron diffraction patterns, with a weighing scheme of 50–50%. For the last compound an impurity was detected. The main peaks of this impurity were found with the interatomic distances d: 3.148, 2.666 and 1.732 Å, as shown in Fig. 4. This leads to a pseudo-Scheelite structure with the composition "$La_{0.66}WO_4$" with quadratic cell parameters of $a = 5.33$ Å and $c = 11.70$ Å. The

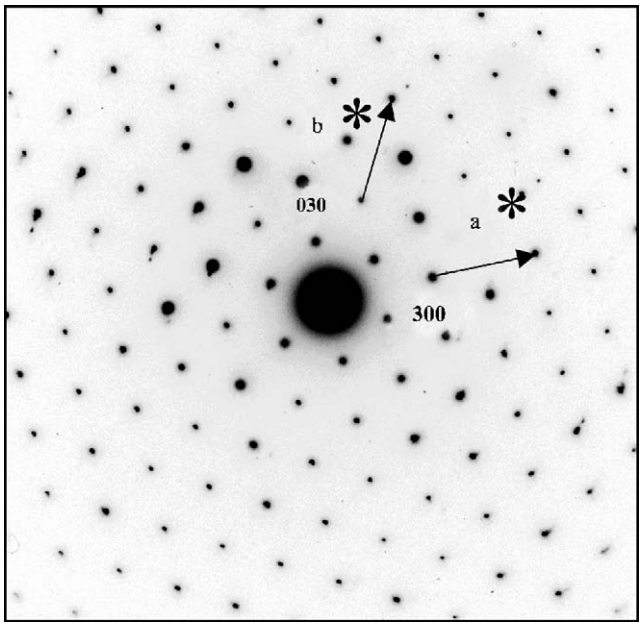

Fig. 2. Electron diffraction pattern of $La_7Ta_3W_4O_{30}$ along [001]* the hexagonal cell.

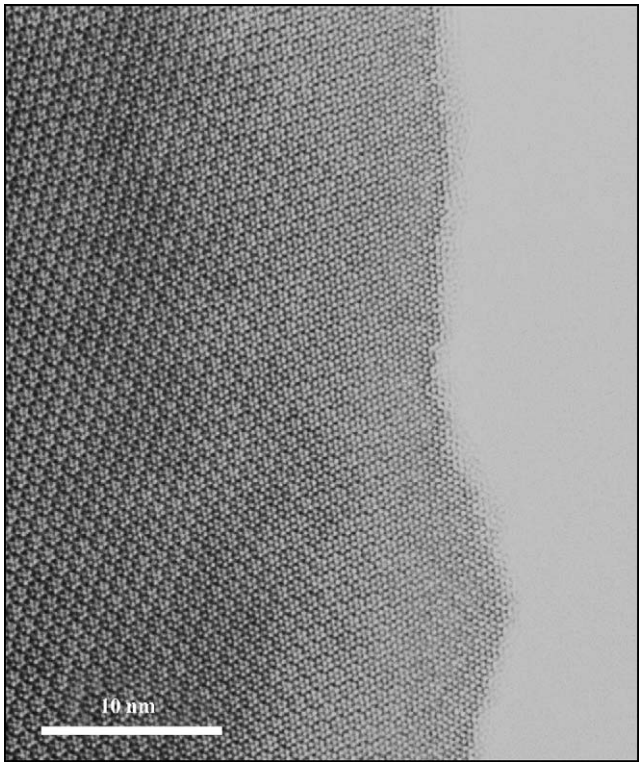

Fig. 3. High resolution electronic images of $La_7Ta_3W_4O_{30}$ along [001], a very periodic contrast is observed in all the crystal attesting of the nice ordering of the structure.

quantitative analysis of this impurity was calculated by the Rietveld method, it gave for the X-ray pattern a weighted fraction of 5.1(3)%. The quality of this last result is poor due to the difficulty to have a realistic knowledge of the real composition of this phase. For $La_7Ta_3W_4O_{30}$, such an impurity was not detected, only few tiny peaks were detected. For both the compounds, the mixed refinements led to a systematic negative value of the thermal agitation factor of the mixed sites W/Nb and W/Ta. Many possibilities of mixing sites were tested on the crystallographic 18*f* and 3*b* sites without success. Finally, we decided to refine the structure only with the neutron diffraction pattern. The crystallographic positions and the thermal agitation factor of $La_7Ta_3W_4O_{30}$ are given in Table 1. The value of the wavelength for the neutron refinements was taken from the mixed refinement, where the wavelength $K\alpha$(Cu) was kept fixed and the neutron wavelength was refined. These final refinements lowered the profile factor R_{wp} to 10.1% and 10.7%, respectively, for $La_7Ta_3W_4O_{30}$ and $La_7Nb_3W_4O_{30}$, the diagrams are presented in Fig. 5a and 5b. For $La_7Nb_3W_4O_{30}$ the refinement leads to quite similar values (see Table 2).

Comparing with the reduced molybdate phase $La_7Mo_7O_{30}$, the final composition of the compounds $La_7A_3W_4O_{30}$ (A = Nb, Ta) is more evident. The consideration of the usual oxidation state of different atoms: La^{+3}, W^{+6}, Nb^{+5} and Ta^{+5} fixes the oxygen composition to 30. Nevertheless, in order to study the relative distribution of the tungsten atoms and the niobium or the tantalum atoms of the both 3*b* and 18*f* sites, different models were tested (see Table 3). The best solution is found when the 3*b* site is occupied by 80% of tantalum. In order to simplify the crystallographic data, we have taken arbitrarily the last model where the 3*b* site is occupied by 100% of tantalum. With this model, the refinement of all the atomic parameters and isotropic thermal factors lowered the refinement factor to $R_{Bragg} = 3.75\%$ and 4.48% for the tantalum and the niobium phase, respectively.

The analysis of interatomic distances and angles (see Table 4) was based on the atomic parameters as refined from the neutron diffraction data on $La_7Ta_3W_4O_{30}$. As for the reduced phase $La_7Mo_7O_{30}$, the La1 and La2 coordination polyhedra are very similar. The La1 coordination polyhedron is a quasi-regular icosahedron, with La1–O3 = 2.56 Å/*2.59 Å* and La1–O5 = 2.73 Å/*2.70 Å*, respectively, for $La_7Ta_3W_7O_{30}$ and *$La_7Mo_7O_{30}$*. The La2 coordination polyhedron is more distorted, La2 being surrounded by nine oxygen atoms at distances ranging from 2.42 to 2.86 Å and *2.44* to *2.85 Å* for *$La_7Mo_7O_{30}$*. As mentioned in a previous paragraph, the occupation on the mixed sites 3*b* and 18*f* by tungsten and tantalum/niobium atoms was not so trivial to predict. Our previous idea was to put the 9 tantalum atoms on the 18*f* site, leading to a 50% occupation with tungsten atoms, and the rest of the tungsten atoms on the 3*b* site. Thus the general formula of 9 tantalum and 12 tungsten atoms was respected. The refinement has given an opposite solution. Analysis of the distortion on the 3*b* and 18*f* crystallographic sites can give an

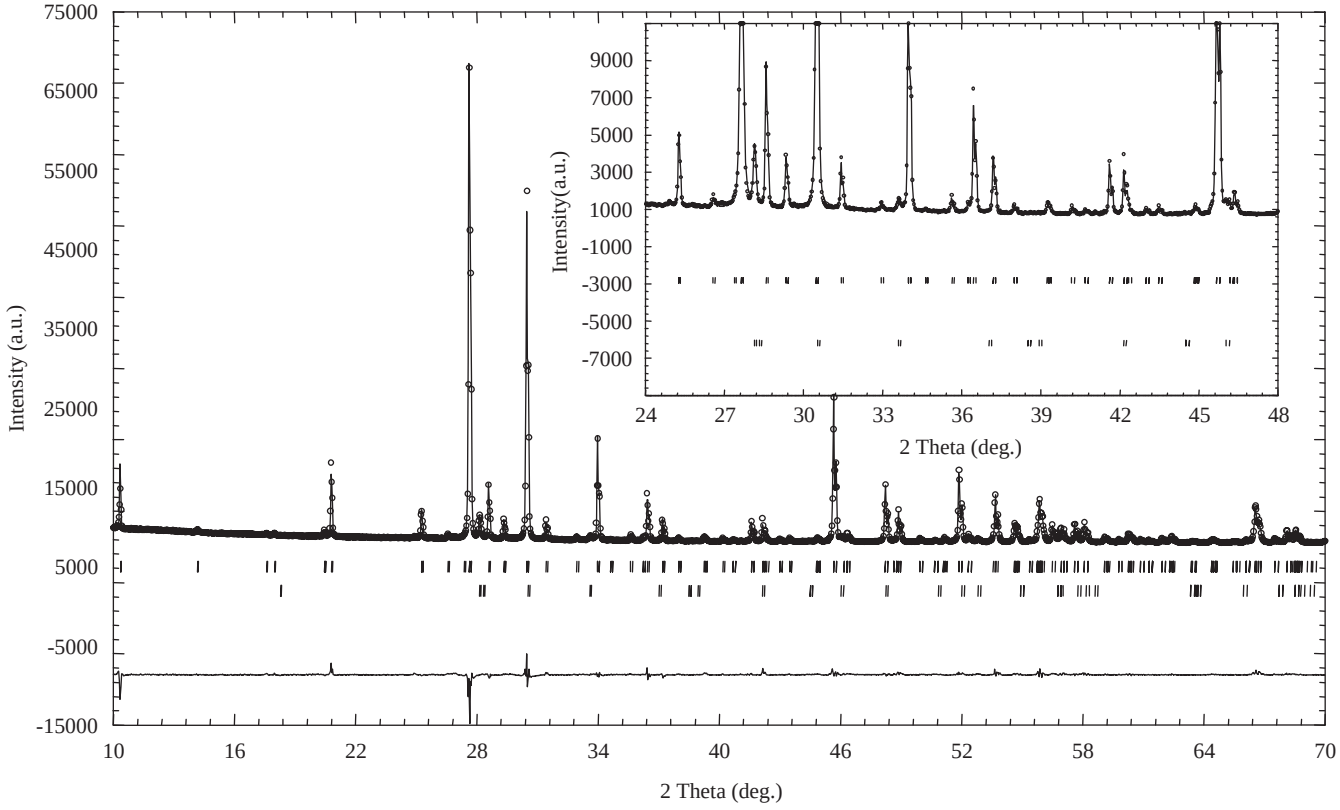

Fig. 4. Part of the final profile X-rays refinements of $La_7Nb_3W_4O_{30}$ (observed (cross), calculated (line) and difference (lower)) profiles is shown. In insert, zoom of a region where the Scheelite impurity is observed as shown.

Table 1
Crystallographic parameters of $La_7Ta_3W_4O_{30}$

Atom	Site	Occupancy	x	y	z	B (Å^2)
La1	3*a*	1	0	0	0	1.0(1)
Ta1	3*b*	1	0	0	0.5	1.3(2)
La2	18*f*	1	0.7766(2)	−0.0173(2)	0.3443(4)	1.16(5)
W2/Ta2	18*f*	0.66/0.33	0.1998(2)	0.0151(2)	0.1596(5)	0.78(5)
O1	18*f*	1	0.2460(2)	0.1006(2)	0.3563(5)	0.86(6)
O2	18*f*	1	0.2930(2)	0.0431(2)	−0.0074(5)	1.22(6)
O3	18*f*	1	0.1691(2)	0.1118(2)	0.0454(5)	1.23(7)
O4	18*f*	1	0.2044(3)	−0.0726(3)	0.3067(4)	1.08(6)
O5	18*f*	1	0.0348(2)	0.1049(2)	0.3237(5)	1.23(6)

Note: Space group *R*-3 (No. 148), $Z = 3$, Cell parameters : $a = 17.0701(2)$ Å, $c = 6.8851(1)$ Å. $R_{wp} = 10.1\%$, $\chi^2 = 7.25$, $R_{exp} = 3.84\%$, $R_B = 3.75\%$ (444 reflections). Calculated density = 7.83 g cm^{-3}, measured density = 7.81(1) g cm^{-3}.

explanation. The atom on the 3*b* site presents a coordination polyhedron, which is an almost regular octahedron with no distortion. On the contrary, the 18*f* site presents a coordination polyhedron which is more distorted with a distortion of 62×10^4. The maximum distortion found for Mo^{+6},W^{+6}, Nb^{+5} and Ta^{+5}, is respectively, 212, 122, 83 and 79×10^4, from Shannon [11]. From this remark, we can assume that the niobium and tantalum atoms will preferred less distorted environment; consequently, the 3*b* site is first fully occupied by these atoms.

The Ta1 coordination polyhedron is formed by six oxygen atoms at 1.99 Å. This value has to be compared with the Mo1–O5 distance in which is also 1.99 Å $La_7Mo_7O_{30}$. The Ta2/W2 coordination polyhedron is formed with the metal–oxygen distances from 1.82 to 2.24 Å, respectively, 1.77 to 2.21 Å for $La_7Mo_7O_{30}$.

The bond valence sum calculation were performed directly in the Fullprof program [12], by using the Brown–Altermatt empirical expression: Valence = $\Sigma\exp(R_0-d)/B$ with $B = 0.37$ Å [13]. The values used

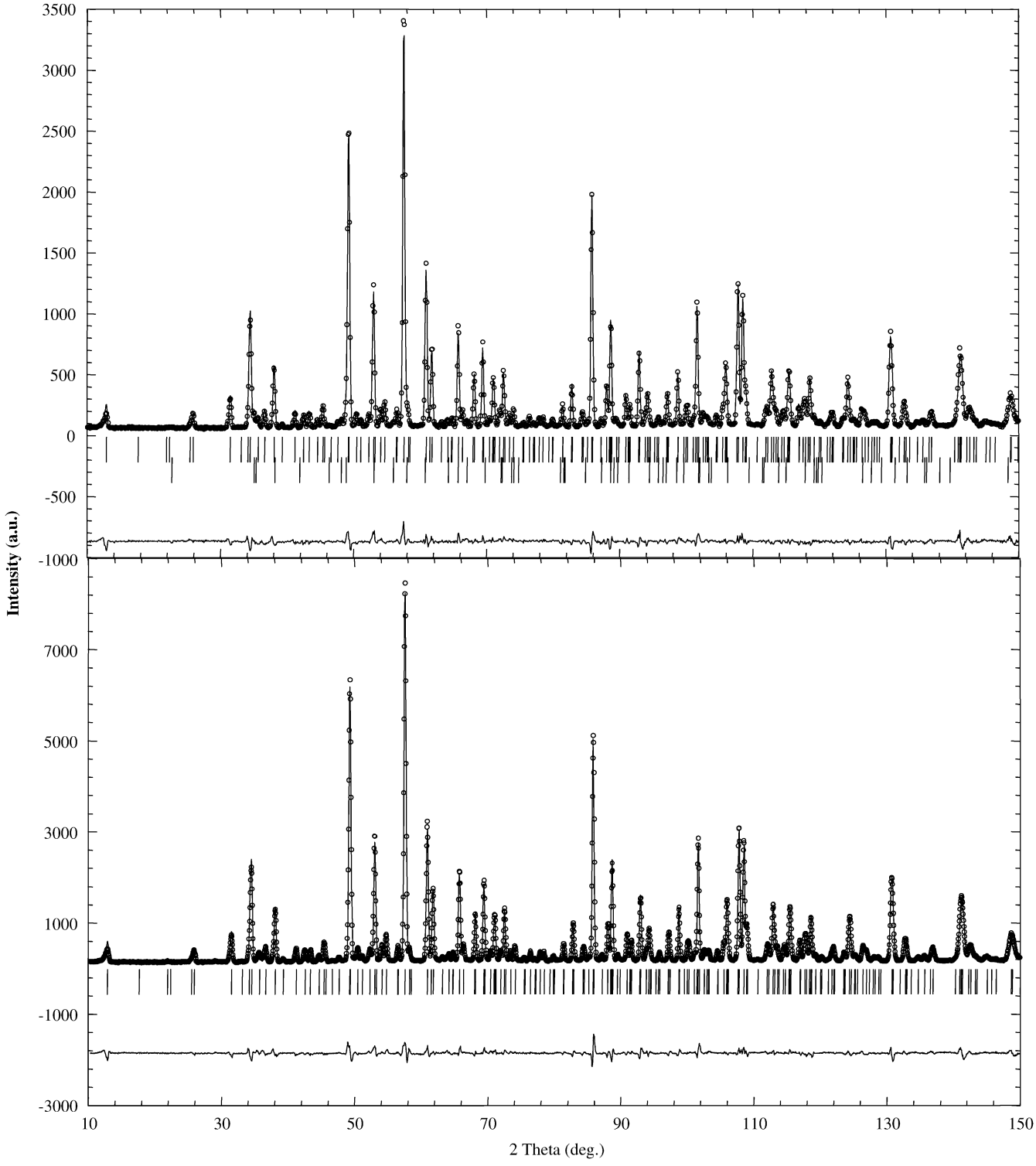

Fig. 5. Neutron refinements for: (top) $La_7Nb_3W_4O_{30}$ and (bottom) $La_7Ta_3W_4O_{30}$.

by the Fullprof program were for La^{3+}–O^{2-} $R_0 = 2.172$ Å, Ta^{5+}–O^{2-} $R_0 = 1.920$ Å and for W^{6+}–O^{2-} $R_0 = 1.921$ Å. The bond valence sum calculation (BVS see Table 5), for the lanthanum atoms gives values slightly in excess of the expected +3: 3.41 and 3.04, respectively, for La2 and La1, which are comparable with 3.35 and 3.08 obtained for $La_7Mo_7O_{30}$. Such values of BVS ≈ 3.4 for the lanthanum atom is rather usual in lanthanum molybdates or tungstate, for instance, in $La_2Mo_4O_{15}$ structure [14]: 3.44(4) and 3.17(4) for the

Table 2
Crystallographic parameters of $La_7Nb_3W_4O_{30}$

Atom	Site	Occupancy	x	y	z	B (Å^2)
La1	3*a*	1	0	0	0	0.9(2)
Nb1	3*b*	1	0	0	0.5	1.9(2)
La2	18*f*	1	0.7773(2)	−0.0170(2)	0.3445(4)	0.88(5)
W2/Nb2	18*f*	0.66/0.33	0.2008(2)	0.0154(2)	0.1595(3)	0.36(6)
O1	18*f*	1	0.2458(2)	0.1003(3)	0.3550(2)	0.89(7)
O2	18*f*	1	0.2935(2)	0.0433(2)	−0.0079(2)	1.03(7)
O3	18*f*	1	0.1689(3)	0.1127(3)	0.0445(2)	1.08(7)
O4	18*f*	1	0.2045(3)	−0.0721(3)	0.3054(2)	0.86(6)
O5	18*f*	1	0.0351(2)	0.1047(2)	0.3245(2)	1.05(7)

Note: Space group *R*-3 (No. 148), Z = 3, Cell parameters : $a = 17.0640\ (2)$ Å, $c = 6.8859\ (1)$ Å. $R_{wp} = 10.7\%$, $\chi^2 = 3.46$, $R_{exp} = 5.80\%$, $R_B = 4.48\%$ (450 reflections). Calculated density = 7.08 g cm^{-3}, measured density = 7.03(1) g cm^{-3}.

Table 3
Result of Bragg refinement factor versus different percentages of Tantalum on the 3*b* crystallographic site for $La_7Ta_3W_4O_{30}$

Tantalum (%)	R_{Bragg} (%)
0	4.339
20	4.180
40	4.081
60	4.024
80	4.000
100	4.050

Table 4
Selected bond distances (Å) for $La_7Ta_3W_4O_{30}$

(La1)–(O3): 2.562(4) (× 6)	(Ta1)–(O5): 1.992(4) (× 6)
(La1)–(O5): 2.731(4) (× 6)	
	(W2/Ta2)–(O1): 1.853(5)
(La2)–(O1): 2.508(4)	(W2/Ta2)–(O2): 1.822(5)
(La2)–(O1): 2.423(4)	(W2/Ta2)–(O3): 1.981(5)
(La2)–(O2): 2.542(4)	(W2/Ta2)–(O4): 1.841(5)
(La2)–(O2): 2.493(5)	(W2/Ta2)–(O3): 2.117(5)
(La2)–(O3): 2.656(5)	(W2/Ta2)–(O5): 2.241(5)
(La2)–(O4): 2.860(5)	
(La2)–(O4): 2.781(4)	
(La2)–(O5): 2.509(5)	
(La2)–(O5): 2.598(5)	

Table 5
Calculated bond valence for $La_7Ta_3W_4O_{30}$

Atom	Calculated valence	Atom	Calculated valence
La1	3.03(2)	O1	2.11(2)
La2	3.41(1)	O2	2.09(2)
Ta1	4.94(2)	O3	2.06(2)
W2/Ta2	5.60(3)	O4	1.99(2)
		O5	1.78(1)

two lanthanum atoms, in $La_6Mo_8O_{33}$ [15]: 3.0(1), 3.4(1), 3.1(1), 3.1(1), 3.4(1) and 3.1(1), in $La_2W_2O_9$ [16]: 3.30 and 2.89 and in $Pr_2Mo_6O_{21}\cdot H_2O$ [17]: 3.6 and 3.3 for the praseodynium atoms.

For Ta1 the bond valence calculation leads to a value close to +5. For the mixed site the bond calculation gives +5.60, which is close to the perfect value +5.66 deduced by the occupation $6Ta^{+5} + 12W^{+6}$.

This solution shows a small difference with the one found for $La_7Mo_7O_{30}$, where the valences of two sites Mo1 and Mo2 are +4.5 and +5.75, respectively. Here, the valence of the two sites Ta1 and W2/Ta2 is +5 and +5.6. In order to decrease the valence of the Ta1 site the only solution is to modify the stoichiometry in the oxygen atoms. This can be done if the compound presents a solid solution in the low content of $LaWO_{4.5}$. But, Cava et al. have mentioned that this compound do not present a long range of stoichiometry. We also found no evidence of such solid solution, and the compound should be considered as stoichiometric with the formula A7B7X30.

The two new compounds $La_7A_3W_4O_{30}$ (A = Nb, Ta) really confirm this new structural type: $A_7B_7X_{30}$. This structure is built up from an hexagonal stacking of isolated perovskite-type building units. Contrary to other perovskite-related structures [18], with axes of building units along the perovskite [100] direction, the building units are here cylinders along the perovskite [111] axis (see Fig. 6).

3.4. Impedance and thermal expansion measurements

The two new compounds $La_7A_3W_4O_{30}$ (A = Nb, Ta) are isostructural to $La_7Mo_7O_{30}$. The last compound has been reformulated in $La_2Mo_2O_{8.57}$, which is the reduced phase of the fast oxide-ion conductor $La_2Mo_2O_9$. This proximity is incited us to study the ionic conduction of $La_7A_3W_4O_{30}$ by mean of impedance spectroscopy. Contrary to other phases in the La_2O_3–MoO_3 system [16], which present in general nice semi-circle in the Nyquist plot, the measurement on $La_7Ta_3W_4O_{30}$ gives straight vertical lines at all temperatures (400–1000 °K). Such straight vertical lines were simulated by a capacitance with a constant value close to $\varepsilon_r \approx 20$.

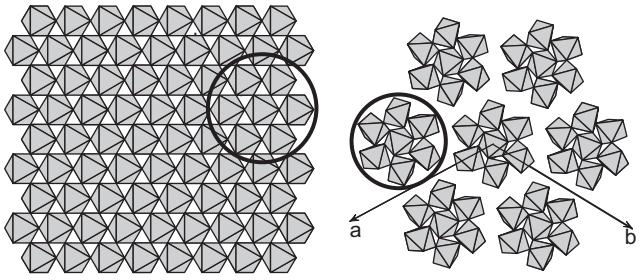

Fig. 6. Projection of the perovskite structure and $La_7A_3W_4O_{30}$ structure along [111] and [001], respectively.

Thermal expansion coefficients were measured using the thermal X-rays diffraction in the range of 30–1000 °C with intermediate points (200, 400, 600 and 800 °C). For both the compounds $La_7A_3W_4O_{30}$ (A = Nb, Ta), the cell parameters linearly increase, the calculated thermal expansion coefficients $\alpha_{30,1000}$ are 11.3 and 11.2×10^{-6}, respectively, for Ta and Nb.

4. Conclusion

The crystallographic structure of a reported compound of formula $LaNb_{0.4}W_{0.6}O_{4.3}$ (60% of $LaWO_{4.5}$ in the phase diagram $LaNbO_4$–$LaWO_{4.5}$) has been solved. This compound presents a slightly different composition 57.1% of $LaWO_{4.5}$ and it should be formulated as $La_7Nb_3W_4O_{30}$. Two compounds $La_7A_3W_4O_{30}$ (A = Nb, Ta) have been synthesized and analyzed. The structure of $La_7A_3W_4O_{30}$ (A = Nb, Ta) has been found to be isostructural of the reduced molybdate compound $La_7Mo_7O_{30}$. This is the first example of such an isotype, in fact the reduced molybdate ($Mo^{+5.57}$) could be simulated by a mixing of (A^{5+}/W^{6+}). An order in the A^{5+} and W^{6+} distribution has been observed, and explained by the analysis of the distortion of different crystallographic sites. The compounds do not present any ionic conduction property. An attempt to obtain such a phase with molybdenum was unsuccessful.

Reference

[1] S.J. Skinner, J.A. Kilner, Mater. Today 1 (2003) 30–37.
[2] P. Lacorre, F. Goutenoire, O. Bohnke, R. Retoux, Y. Laligant, Nature 404 (2000) 856–858.
[3] F. Goutenoire, O. Isnard, R. Retoux, P. Lacorre, Chem. Mater. 12 (2000) 2575–2580.
[4] J.E.H. Sansom, D. Richings, P.R. Slater, Solid State Ionics 139 (2001) 205–210.
[5] T. Esaka, Solid State Ionics 52 (1992) 319–325.
[6] S. Takai, S. Touda, K. Oikawa, K. Mori, S. Torii, T. Kamiyama, T. Esaka, Solid State Ionics 148 (2002) 123–133.
[7] S.J Skinner, Solid state Ionics 154-155 (2002) 325–329.
[8] S. Uma, R. Bliesner, A.W. Sleight, Solid State Sci. 4 (2002) 329–333.
[9] R.J. Cava, R.S. Roth, T. Negas, H.S. Parker, D.B. Minor, J. Solid State Chem. 40 (1981) 318–329.
[10] F. Goutenoire, R. Retoux, E. Suard, P. Lacorre, J. Solid State Chem. 142 (1999) 228–235.
[11] R.D. Shannon, Acta Crystallogr. A 32 (1976) 751–767.
[12] J. Rodriguez-Carvajal, in: Collected Abstracts of Powder Diffraction Meeting, Toulouse, France, 1990, p. 127.
[13] I.D. Brown, D. Altermatt, Acta Crystallorg. B 41 (1985) 244.
[14] F. Dubois, F. Goutenoire, Y. Laligant, E. Suard, P. Lacorre, J. Solid State Chem. 159 (2001) 228–233.
[15] V. Brizé, S. Georges, S. Kodjikian, E. Suard, F. Goutenoire, J. Solid State Chem. 177 (2004) 2617–2627.
[16] Y. Laligant, A. Le Bail, F. Goutenoire, J. Solid State Chem. 159 (2001) 223–227.
[17] H. Naruke, T. Yamase, J. Solid State Chem. 178 (2005) 702–708.
[18] R.H. Mitchell, Perovskites, modern and ancient, Almaz Press Inc., 2002.